

AD-A273 681



ARMY RESEARCH LABORATORY



Correlation of the Failure Modulus  
to Fracture-Generated Surface Area  
in Uniaxially Compressed  
M30 Gun Propellant

— Robert J. Lieb  
Michael G. Leadore

ARL-TR-307

November 1993



APPROVED FOR PUBLIC RELEASE; DISTRIBUTION IS UNLIMITED.

93-30124



93 12 10 026

## NOTICES

Destroy this report when it is no longer needed. DO NOT return it to the originator.

Additional copies of this report may be obtained from the National Technical Information Service, U.S. Department of Commerce, 5285 Port Royal Road, Springfield, VA 22161.

The findings of this report are not to be construed as an official Department of the Army position, unless so designated by other authorized documents.

The use of trade names or manufacturers' names in this report does not constitute endorsement of any commercial product.

BEST AVAILABLE COPY

# REPORT DOCUMENTATION PAGE

Form Approved  
OMB No. 0704-0188

Public reporting burden for this collection of information is estimated to average 1 hour per response, including the time for reviewing instructions, searching existing data sources, gathering and maintaining the data needed, and completing and reviewing the collection of information. Send comments regarding this burden estimate or any other aspect of this collection of information, including suggestions for reducing this burden, to Washington Headquarters Services, Directorate for Information Operations and Reports, 1215 Jefferson Davis Highway, Suite 1204, Arlington, VA 22202-4302, and to the Office of Management and Budget, Paperwork Reduction Project(0704-0188), Washington, DC 20503.

1. AGENCY USE ONLY (Leave blank)		2. REPORT DATE November 1993		3. REPORT TYPE AND DATES COVERED Final Nov 92 - Apr 93	
4. TITLE AND SUBTITLE Correlation of the Failure Modulus to Fracture-Generated Surface Area in Uniaxially Compressed M30 Gun Propellant				5. FUNDING NUMBERS PR: 1L161102AH43	
6. AUTHOR(S) Robert J. Lieb and Michael G. Leadore					
7. PERFORMING ORGANIZATION NAME(S) AND ADDRESS(ES) US Army Research Laboratory ATTN: AMSRL-WT-PE Aberdeen Proving Ground, MD 21005-5066				8. PERFORMING ORGANIZATION REPORT NUMBER	
9. SPONSORING/MONITORING AGENCY NAME(S) AND ADDRESS(ES) US Army Research Laboratory ATTN: AMSRL-OP-CI-B (Tech Lib) Aberdeen Proving Ground, MD 21005-5066				10. SPONSORING/MONITORING AGENCY REPORT NUMBER ARL-TR-307	
11. SUPPLEMENTARY NOTES				Accession For	
				NTIS CRA&I <input checked="" type="checkbox"/> DTIC TAB <input type="checkbox"/> Unannounced <input type="checkbox"/> Justification	
12a. DISTRIBUTION/AVAILABILITY STATEMENT Approved for public release; distribution is unlimited				12b. DISTRIBUTION CODE	
				By _____ Distribution / _____ Availability Codes Dist Avail and/or Special A-1	
13. ABSTRACT (Maximum 200 words) M30, a triple base large caliber propellant, was uniaxially compressed at a rate of 100/s to an end state strain of 50.0%, 20.0%, and 10.0% at temperatures from -40 to 60 degrees C. The failure modulus was measured, and closed bomb firings were made to determine how the grain damage affected the pressure generation. The pressure-time curves from the damaged propellant were analyzed to extract the burning surface area profiles. Results showed that a line fit to the first 10% of the surface area versus fraction burned curve seemed to be directly related to the logarithm of the failure modulus. The three resulting least square fit curves, one for each level of strain, fell into a series that permitted the effective surface area profile to be predicted for any combination of failure modulus and end state strain within the fracture domain. These results provide a method for assessing fracture damage by means of a simple mechanical measurement.					
14. SUBJECT TERMS mechanical response, surface area, fracture damage, propellants, M30, failure modulus, failure				15. NUMBER OF PAGES 26	
				16. PRICE CODE	
17. SECURITY CLASSIFICATION OF REPORT UNCLASSIFIED	18. SECURITY CLASSIFICATION OF THIS PAGE UNCLASSIFIED	19. SECURITY CLASSIFICATION OF ABSTRACT UNCLASSIFIED	20. LIMITATION OF ABSTRACT SAR		

**Intentionally Left Blank**

## TABLE OF CONTENTS

	<u>Page</u>
LIST OF FIGURES .....	v
LIST OF TABLES .....	v
1. INTRODUCTION .....	1
2. EXPERIMENTAL PROCEDURE .....	2
2.1 Mechanical Response Measurement .....	2
2.2 Fracture-Generated Surface Area Measurements .....	3
2.3 Details of the Experiment .....	4
3. RESULTS .....	4
4. ANALYSIS .....	6
4.1 Statement of the Problem .....	6
4.2 Method of Analysis .....	8
4.3 Results of Analysis .....	8
5. DISCUSSION .....	11
5.1 Use of Equations .....	11
5.2 Observations from Low Fracture Results .....	12
6. CONCLUSIONS .....	13
7. FUTURE STUDIES .....	14
8. REFERENCES .....	15
DISTRIBUTION LIST .....	17

**Intentionally Left Blank**

## LIST OF FIGURES

<u>Figure</u>	<u>Page</u>
1    Servohydraulic Tester.....	2
2    Mechanical Characterization Parameters .....	3
3    Stress vs. Strain Response Curves for M30 from which Failure Modulus Values are Determined .....	5
4    Ln of the Failure Modulus of M30 Propellant vs. Temperature over the Temperature Range of Ballistic Interest.....	5
5    Photographs of the M30 Propellant Specimens after Compression to 50% Strain ...	5
6    Theoretical and Undamaged Values of the Surface Area Ratio vs. Fraction Burned .....	6
7    Surface Area Profiles at Selected Temperatures for Propellant Damaged at 50% Strain Figure.....	6
8 $S/S_0$ vs. Fraction Burned for Grains Damaged under Different Conditions.....	7
9    Average $S/S_0$ vs. Fraction Burned Curves with Least Squared Best Fit Lines .....	9
10   Least Squares Fit Parameters vs. Ln of the Failure Modulus of $S/S_0$ vs. Fraction Burned for Each Strain .....	10
11   Parameters from Fitting Equations in Figure 10 vs. End-Strain Figure .....	11
12   Surface Area vs. Fraction Burned for M30 Propellant with Low Fracture Response .....	13
13   M30 Propellant Grains Compressed to 20% Strain at 20 °C .....	13

## LIST OF TABLES

<u>Table</u>	<u>Page</u>
1    M30 Nominal Percent Composition .....	2
2    Average Values of Failure and Surface Area Ratio Parameters .....	10

**Intentionally Left Blank**

## 1. INTRODUCTION

Attempts to establish the relationship between mechanical measurements and gun performances have made steady progress in the past 5 years<sup>1-13</sup>. Early work revealed that conventional mechanical parameters did not relate well to fracture susceptibility. The search for a simple mechanical parameter that could measure the propensity of a propellant to generate surface area upon mechanical failure resulted in the development of a failure parameter called the failure modulus<sup>4</sup>,  $E_f$ , that measures the rate at which the material strength is lost as a function of strain, after failure has occurred. This parameter has been used as a guide in the development of new propellants to ensure that improvements in formulation and processing did not degrade the mechanical response characteristics of the material, which could result in poor performance and increased vulnerability response. This parameter has also been successfully used to evaluate the relative fracture susceptibility among several propellant lots or between unconditioned propellant and propellant that has been subjected to conditioning, such as thermal cycling, that may affect its mechanical response.

This parameter showed indications of direct usefulness when the changes of the vulnerability response related directly to the changes measured in this failure parameter<sup>3</sup>. The correlation was found for propellant beds at low temperature subject to a shaped charge jet attack and led to other studies that attempted to make the correlation more direct. However, the relationship was made between changes in both responses, rather than directly relating the responses themselves.

In this study, a direct link between this parameter and a measure of the amount of fracture-generated surface area produced during uniaxially compression is made for M30 propellant. Measurement of the failure modulus was made on the grains, and enough grains were damaged so that closed bomb firings could be made to determine how the grain damage affects the pressure generation under ballistic pressures. A small (21 cc) closed bomb was used so that large numbers of grains did not have to be damaged to reach gun-like pressures in the closed vessel. After the burning rate using undamaged grains was established, the pressure-time curves from the damaged propellant were analyzed for surface area. Many attempts were made to establish a method for analyzing the closed bomb data. As proper considerations became clearer, modifications of the analysis were made, which resulted in a method that relates the augmentation of pressure generation to the failure modulus and the level of strain suffered by the M30 propellant.

The question of the use of uniaxial response measurements to link a mechanical parameter of a propellant grain to the aggregate behavior within gun systems must be addressed. Certainly, the system is complex and the system elements are nonlinear. The success of linking a simple testing

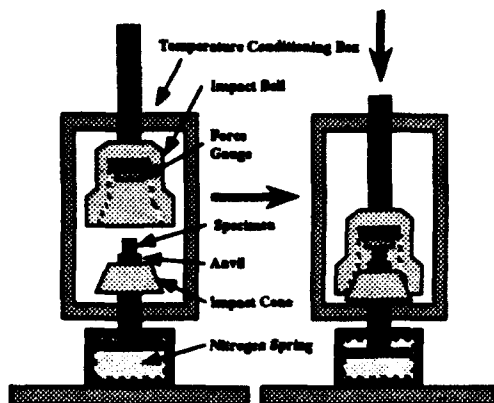


Figure 1. Servohydraulic Tester

Table 1. M30 Nominal Percent Composition

Component	Percent Composition
Nitrocellulose (NC)	28
NC Nitration Level	12.6
Nitroglycerin (NG)	22
Nitroguanidine (NQ)	48
Ethyl Centralite (EC)	2

procedure to a complex event will depend upon the ability to extract from the uniaxial response an essential indicator of fracture behavior within the system. As of yet, this has not been demonstrated. However, indications are from the examples cited above that the propellant response seems robust enough to provide some guidance for using these measurements as such an indicator. Attempts are under way to link the grain and aggregate mechanical response in a way to predict bed behavior from grain response and size. As more information is extracted from the response measurements, the ability to predict will become clearer.

## 2. EXPERIMENTAL PROCEDURE

**2.1 Mechanical Response Measurement** The propellant response was measured using a specially designed servohydraulic tester<sup>5</sup>, illustrated in Figure 1. The machine allows for compression measurements to be performed at rates as great as  $1000 \text{ s}^{-1}$  for a specimen with a nominal length of 1 cm. Compression is arrested when contact occurs between the impact bell and cone. Therefore, the amount of specimen compression can be accurately predetermined by setting the anvil height. This contact between bell and cone not only stops the specimen compression, but it also shunts the force around the specimen. The nitrogen spring absorbs the decelerating force of the massive ram and extends its duration. The force applied to the specimen is measured using the gauge inside the impact bell. During compressive response measurements, displacement is measured with a linear variable differential transformer (LVDT) in the actuator column and is corrected for machine stiffness.

The specimens were prepared from multiperforated M30 gun propellant grains whose formulation is listed in Table 1. Specimen preparation procedure began by cutting the sample with a diamond saw to a length of 1.00 cm. The ends were cut flat, parallel and perpendicular to the grain axis according to the specifications in a proposed NATO draft Standard Agreement entitled "Uniaxial

Compressive Test," which is an updated version of the test entitled "Uniaxial Compressive Gun Propellant Test" in the Chemical Propulsion Information Agency Publication 21. Temperature conditioning was achieved by placing prepared grains inside the environmental chamber for a time at least twice that needed to reach thermal equilibrium (30 minutes in most cases). The specimen was then placed on the anvil and tested. This testing took place within the conditioning chamber, so no transfer was required, and therefore, no thermal disruption occurred.

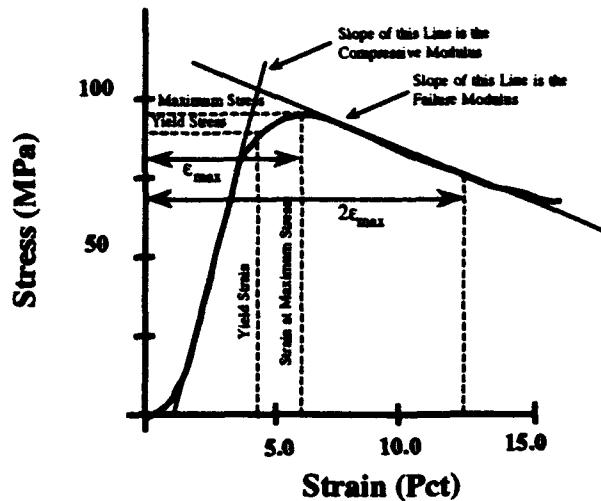


Figure 2. Mechanical Characterization Parameters

The final strain to which the specimen was taken was determined by the distance between the anvil and the force gauge when the bell and cone surfaces were mated. That distance was determined by placing a lead specimen on the anvil and performing a compression. This allowed for any dynamic effects to be taken into account that may have been overlooked in a static measurement. The percentage strain used in these tests was selected to be 50%, 20%, and 10%. From previous testing, it is known that failure of the grain occurs between 3% and 5%, depending upon strain rate and temperature.

The parameters measured in a response characterization test are the modulus, maximum stress, strain at maximum stress, stress at failure, strain at failure, and failure modulus. These parameters are illustrated in Figure 2. The failure modulus is the slope of the stress-strain curve in the near linear region between strain at maximum stress, and twice that value. If no maximum stress occurs in the region of failure, the failure modulus is measured between the strain at failure and three times that value. Measurement of the failure modulus was made at  $-40^{\circ}\text{C}$ ,  $-20^{\circ}\text{C}$ ,  $0^{\circ}\text{C}$ ,  $20^{\circ}\text{C}$ ,  $40^{\circ}\text{C}$ , and  $60^{\circ}\text{C}$ , and the reported values were determined from the average of five response curves. The specimen strain rate was chosen to be  $100\text{ s}^{-1}$ , which is the order of strain rate encountered by the grains during a normal ballistic firing.

**2.2 Fracture-Generated Surface Area Measurement** The grains that were damaged by uniaxial compression, as outlined above, were burned in a mini-closed bomb (MCB) to determine the effect that the mechanical damage had on the pressure generation of the propellant. The MCB is a special, small volume closed bomb<sup>6</sup>. The rate of pressurization during combustion is controlled by the

intrinsic burning rate of the propellant and the surface area exposed to the flame. This enables the surface area to be determined once the burning rate of the propellant has been established.

Undamaged specimens were burned in the MCB at the same loading density that was used in the damaged grain firings. These pressure-time traces were analyzed using the closed bomb reduction code BRLCB<sup>14</sup> to establish the burning rates for the M30 propellant for these tests. Once established, the surface area from all the pressure-time histories can be determined using the same code. The output from the code provides pressure in MPa and the corresponding surface area in square centimeters. This output was converted to intrinsic parameters of fraction burned and surface area ratio ( $S/S_0$ ), respectively, by dividing the pressure by the maximum pressure and the surface area by the initial surface area of the undamaged grain. This permitted closed bomb runs with different charges, pressures, etc., to be compared.

**2.3 Details of the Experiment** Enough grains were damaged to provide two or three closed bomb firings for each temperature-strain condition. Initial tests done at 50% strain had three repetitions performed. Indications from that set of tests were that two closed bomb firings could be performed with reasonable assurance of agreement. If results varied significantly, subsequent tests were performed to resolve the differences. With six temperatures and three end-strain conditions, a total of 46 closed bomb tests were conducted. These included some instances when more than three firings were performed to verify the repeatability of the process.

### 3. RESULTS

The uniaxial compressive mechanical response of M30 propellant is shown in the stress vs. strain curves presented in Figure 3. From these curves, the failure modulus was calculated as outlined above. The resulting values of failure modulus are shown in Figure 4 in which the natural logarithm ( $\ln$ ) of these values is plotted against temperature to show the nature of the response. From these plots, the indication is that fracture becomes rapidly more significant at lower temperatures. This was confirmed by the physical appearance of the grains after testing. Figure 5 shows typical 50% strain specimens after uniaxial compression. The failure modulus values reflected the increase in fracture observed in the tested specimens, but more importantly,  $E_f$  quantified it. This observation prompted the application of this parameter to the characterization of the effect that damage has on the burning of propellant.

For each closed bomb firing, a surface area ratio vs. fraction burned plot was obtained, as described above, which reflected the amount of surface area available to the flame throughout the

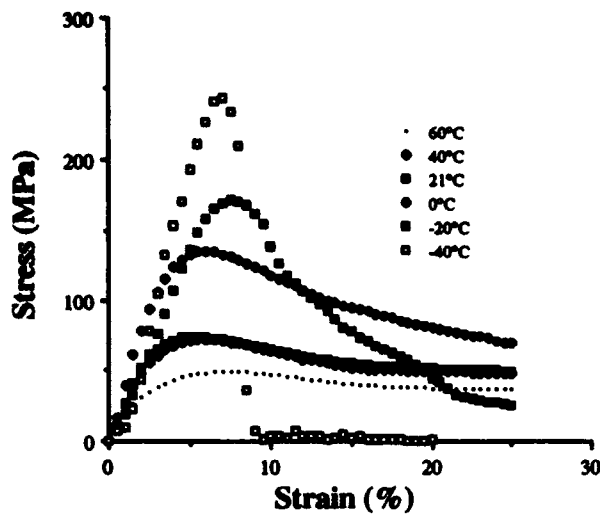


Figure 3. Stress vs. Strain Response Curves for M30 from which Failure Modulus Values are Determined

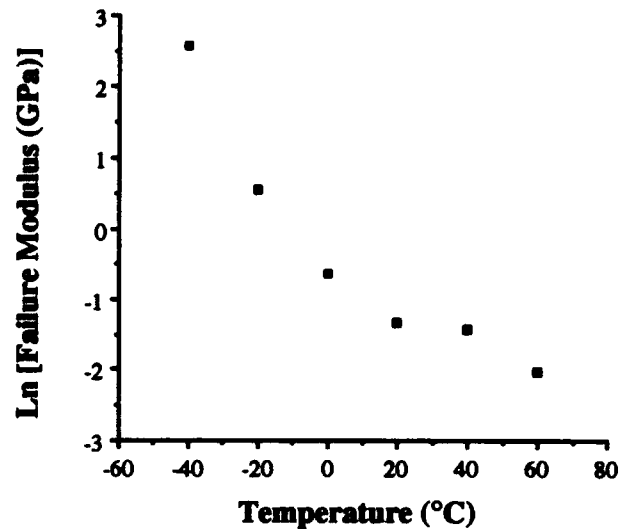


Figure 4. Ln of the Failure Modulus of M30 Propellant vs. Temperature over the Temperature Range of Ballistic Interest



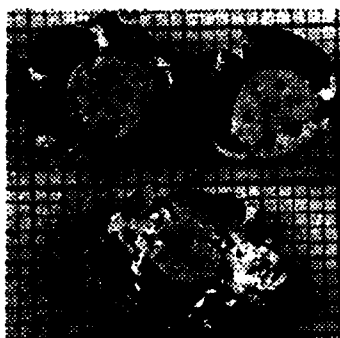
a. -40°C



b. -20°C



c. 0°C



d. 21°C



e. 40°C



f. 60°C

Figure 5. Photographs of the M30 Propellant Specimens after Compression to 50% Strain (1-mm Divisions)

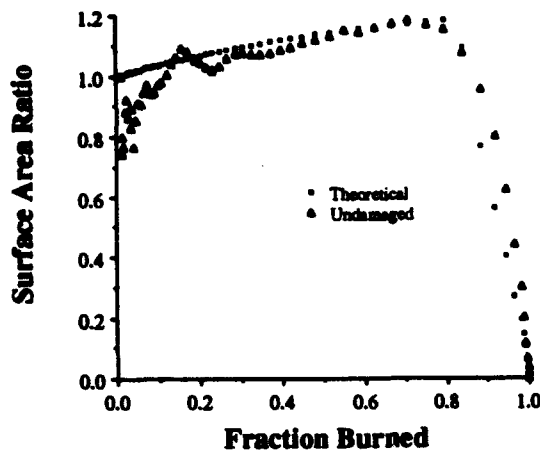


Figure 6. Theoretical and Undamaged Values of the Surface Area Ratio vs. Fraction Burned

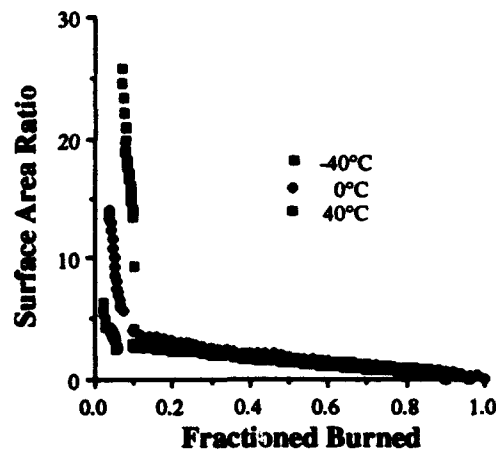
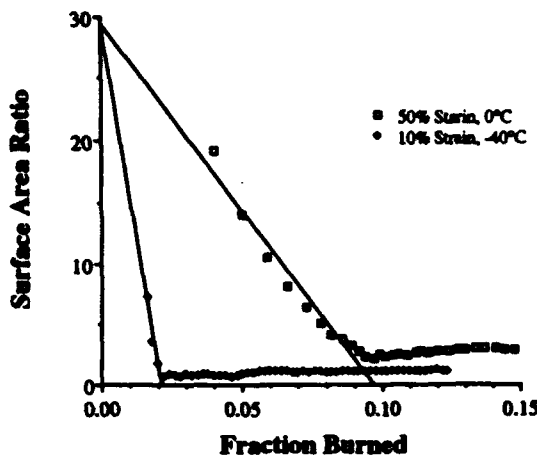


Figure 7. Surface Area Profiles for Propellant Damaged at 50% Strain

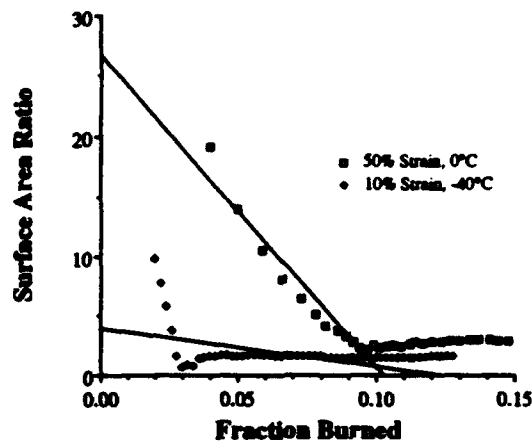
propellant combustion. Figure 6 shows the theoretical and typical experimental values for the surface area ratio vs. fraction burned for undamaged grains. Note that as the seven-perforated grains burned, the surface area increased. This area profile is required to provide the gun with the designed performance. Any deviation from this profile changes the performance. In cases of grain fracture, the performance is almost always reduced and, in cases of extensive damage, can produce catastrophic gun failure. The surface area profiles shown in Figure 7 show how temperature and strain combine to change the pressure generation because of damaged grains. These deviations from the profile required for efficient gun firing are significant and would cause large pressure variations within the gun. The profiles for each condition were analyzed using the procedure outlined below.

#### 4. ANALYSIS

**4.1 Statement of the Problem** Many attempts were made to associate the surface area curves obtained from the closed bomb results to the failure modulus. In the first attempt, the intercept of the initial values of  $S/S_0$  was used and difficulty was found with the values determined from this approach. Figure 8a illustrates the problem. Here, the intercept of the initial values is shown for two curves that were obtained under drastically different conditions. The curves show that brittle fracture occurred in each case, but the extent of the fracture in the 10% strain test was initially much worse than for the other condition. However, fracture was arrested when compression stopped at 10%. This resulted in many finely fractured particles, because of the increased brittleness at  $-40^\circ\text{C}$  and a large surface area. However, after the initial burning of the fine particles, the remaining particles had much



a. Projection of the Initial Points to the Area Ratio Axis



b. Projection of Points Up to 10% Fraction Burned to the Area Ratio Axis

Figure 8.  $S/S_0$  vs. Fraction Burned for Grains Damaged under Different Conditions

less surface area to present to the flame, and the surface area dropped to significantly lower values at a low fraction burned. The fracture that occurred at  $0^\circ\text{C}$  projected the same initial surface area value, but much more extensive damage occurred because of the larger end strain. A much larger mass of finely fractured particles continued to burn rapidly until almost 10% of the charge was consumed. This condition represents a much more rapid rise in pressure and a much greater deviation in the designed surface area profile. A simple method of accounting for the extent of fracture damage needed to be incorporated into the analysis if it was to reflect not only the initial value of the additional fracture-generated surface area, but also the mass and distribution of the fractured particles.

If information outlined above could be reliably extracted from the individual  $S/S_0$  vs. fraction burned curves, then a link could be established to ballistic performance. Many attempts were tried: curve averaging, a comparison of areas under curves to a certain fraction burned, shifting of curves to match minimum surface area values, primary and secondary  $S/S_0$  curve intercepts, and several other methods. Some of these methods worked well for a particular set of conditions (e.g., constant temperature, or constant end-strain) but failed when applied to the general set of fracture conditions. Much work, which is not detailed here, was done to develop a simple procedure for data analysis. The method that seemed to best characterize the deviation reflected in the curves and was still simple enough to be applied easily is described below.

**4.2 Method of Analysis** As explained above, the initial amount of surface area present is important, and the extent to which that surface area continues to be maintained while the propellant burns is at least as important. It would be desirable to incorporate into a single set of quantitative numbers the degree of pressure generation deviation that can be expected because of fracture damage. To date, the method that best exhibits this information for the conditions used in these tests is to fit the points, to 10% fraction burned, of the  $S/S_0$  vs. fraction burned curve to a least squares fit. If this is performed on the curves in Figure 8a, the intercepts shown in Figure 8b result. Note that the intercept values and the slopes of the curves now seem to reflect a more accurate representation of the effect that the available surface area had on pressure generation.

There are several reasons why this approach reflects critical aspects of pressure generation within the gun. First, the conditions during which significant deviations from planned pressure generation within guns occur are established very early in the ballistic cycle. Thus, it makes sense to use only the information contained in the early burning of the charge, i.e., the first 10%. If surface area variances begin to occur later in the cycle, the performance will be affected, but the chamber volume has increased significantly and is continuing to rapidly expand so that excess pressurization is more difficult to generate than at earlier times. Next, this method also increases the number of points that determine the value to be used to characterize the increased surface area. Those familiar with closed bomb analysis know that the most uncertain values generated in the process are those obtained at low fraction burned. This method of curve fitting eliminates the dependence of the values obtained from being determined by a only few points that lie within the early, uncertain region of fraction burned. However, this early combustion region still is able to influence the parameter values. Finally, by incorporating the points at higher fraction burned (i.e., As great as 10%) the degree by which the fracture-generated surface area is maintained is also taken into account. All these features are exhibited in the examples shown in Figure 8.

**4.3 Results of Analysis** The above analysis procedure was applied to each of the closed bomb data sets. However, to provide equal weight to each portion of the curve between the points being fit, values of  $S/S_0$  were calculated at equal intervals of fraction burned, i.e.,  $\Delta FB = 0.02$ , based on an interpolation between nearest data points. This was necessary because at high surface area, more propellant is consumed per time interval. This resulted in larger fraction burned intervals at lower fraction burned, or a greater density of points within the curve at higher fraction burned. This higher density skewed the weighting of the fitted curve. This procedure also facilitated curve averaging. The specific surface area at each fraction burned for each curve, at the same end-strain and temperature condition, was averaged between the maximum value of  $S/S_0$  and the value of  $S/S_0$  at

0.10 fraction burned. This produced an average curve for that testing temperature and end strain combination. These average curves and the associated least squares fit straight line appear in Figure 9. The intercept and slope values for these lines appear in Table 2 along with the corresponding values of the failure modulus.

If these intercept and slope values are plotted against the logarithm of the failure modulus for each of the end-strain levels, and a linear least squares fit is made to the points, the curves in Figure 10 result. The curves form a series that can be related to the end-strain level by setting the constants and coefficients in the fitting equations to be functions of the end strain. This is done in Figure 11, which shows that the dependence of the fitting parameters on the strain appears to be linear. If the equations shown in Figure 11a are substituted into the relationships developed in Figure 10a, the  $S/S_0$  curve intercept can be represented by

$$S_i/S_0(\epsilon, E_f) = -1.84 + 0.361 \epsilon + (0.392 + 0.116 \epsilon) \ln E_f, \quad (1)$$

which can be used to predict values of effective initial surface area ratio, given the measured failure modulus and the strain.

A similar result can be obtained for the slope of the  $S/S_0$  vs. fraction burned curves. These values also appear in Table 2 and are plotted in Figure 11b. When the same operation is performed on the constants and coefficients of the equations in Figure 10b, the coefficient of the

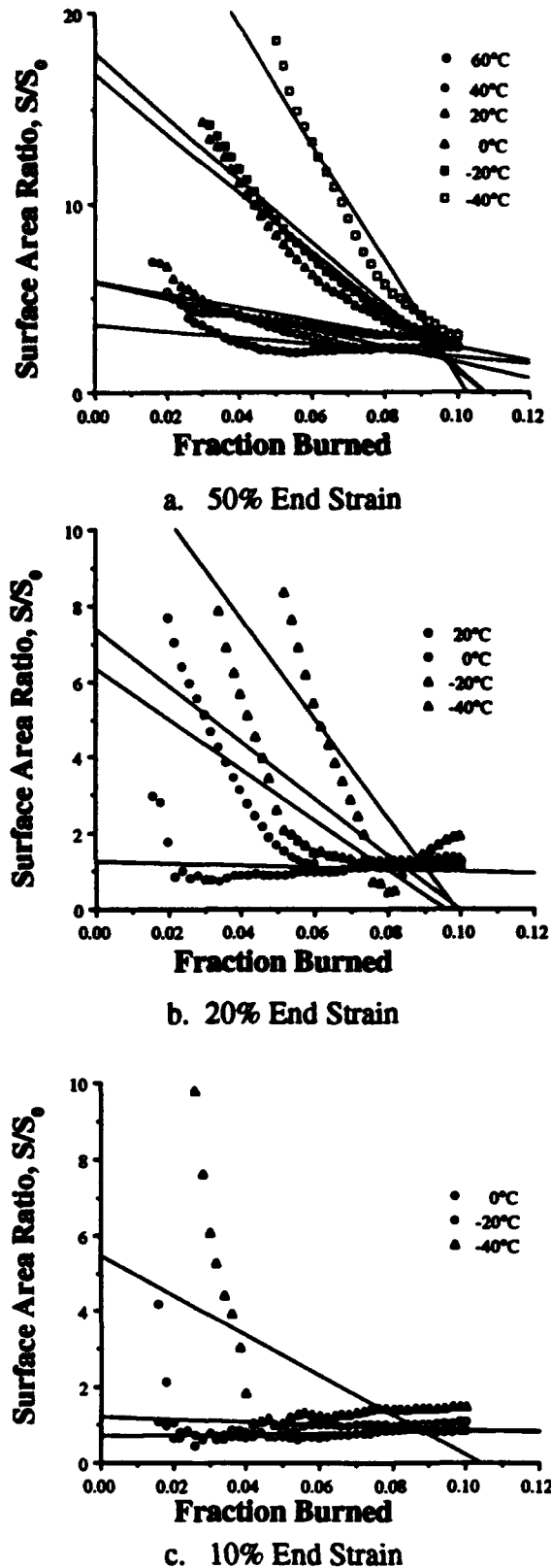
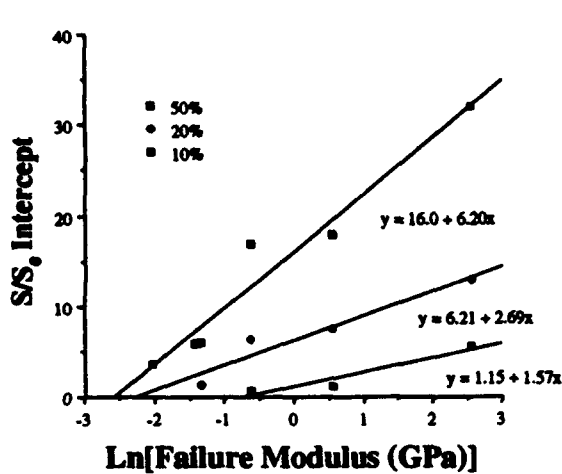


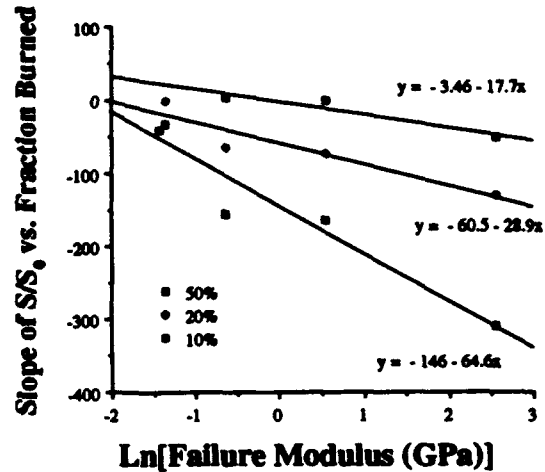
Figure 9. Average  $S/S_0$  vs. Fraction Burned Curves with Least Squared Best Fit Lines

Table 2. Average Values of Failure and Surface Area Ratio Parameters

Temperature (°C)	Failure Modulus ( $E_f$ ) (GPa)	$\ln(E_f)$	Average $S/S_0$ Intercept			Average Slope		
			50%	20%	10%	50%	20%	10%
60.0	0.13	-2.040	3.57	-	-	-16.5	-	-
40.0	0.24	-1.427	5.82	-	-	-42.5	-	-
20.0	0.26	-1.347	5.88	1.26	-	-35.0	-2.9	-
0.0	0.53	-0.635	16.80	6.33	0.67	-157	-66.4	1.48
-20.0	1.74	0.554	17.90	7.37	1.20	-166	-74.1	-3.22
-40.0	12.90	2.557	31.80	12.94	5.41	-310	-131.2	-52.6



a. Surface Area Ratio Intercept



b. Coefficient of Fraction Burned (Slope)

Figure 10. Least Squares Fit Parameters vs.  $\ln$  of the Failure Modulus of  $S/S_0$  vs. Fraction Burned for Each Strain

effective surface area curve can be found by placing the appropriate end-strain and failure modulus values in the following equation:

$$\text{Slope}(\epsilon, E_f) = 20.6 - 3.40\epsilon - (5.71 + 1.18\epsilon) \ln E_f. \quad (2)$$

These two equations can be combined to produce the effective surface area profile vs. fraction burned (usually designated as  $Z$ ) for the first 10% of the fraction burned. This equation appears below:

$$\begin{aligned} S/S_0(\epsilon, E_f, Z) &= S_i/S_0(\epsilon, E_f) + \text{Slope}(\epsilon, E_f) Z \\ &= -1.84 + 0.361\epsilon + (0.392 + 0.116\epsilon) \ln E_f + \\ &\quad [20.6 - 3.40\epsilon - (5.71 + 1.18\epsilon) \ln E_f] Z. \end{aligned} \quad (3)$$

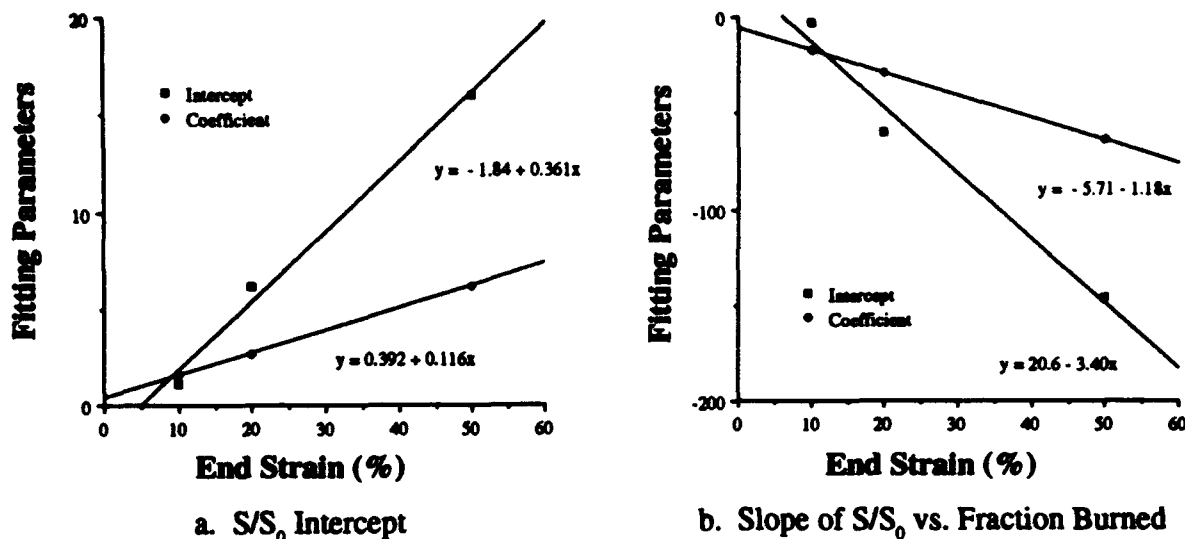


Figure 11. Parameters from Fitting Equations in Figure 10 vs. End Strain

The domain over which these relationships can be expected to apply extends a little beyond the corresponding values for  $\epsilon$  and  $E_f$  for which intercept and slope have been determined in Table 2. The limiting influence is the inability to detect fracture at combinations of low strain and low failure modulus values. There is a greater likelihood of valid results from calculations outside this domain for higher values of  $\epsilon$  and  $E_f$ .

## 5. DISCUSSION

**5.1 Use of Equations** The above equations can be used for several purposes. As stated, if the stress state of the propellant is known and the failure modulus has been measured, then the effect of the initial surface area can be evaluated. The effects of the augmented surface area on combustion for the first 10% of fraction burned can be evaluated by using Equation 3 to predict an effective surface area profile during the early combustion. The prediction may not, however, show the dynamic surface area profile that could affect the generation and propagation of pressure waves within the gun chamber, but it should provide a more accurate assessment of the pressures generated.

Another use of these equations could be to predict when conditions indicate that the fracture-generated surface may become a significant problem. The time-temperature equivalence of M30 and other propellants has been established<sup>10</sup> over the temperature range of ballistic interest and has been related to the strain rate for more than four orders of magnitude<sup>11</sup>. Using this information, one can predict the strain state of a propellant for a certain strain rate deformation at a particular temperature. In the referenced studies, it was shown that the time-temperature equivalency could be extended to

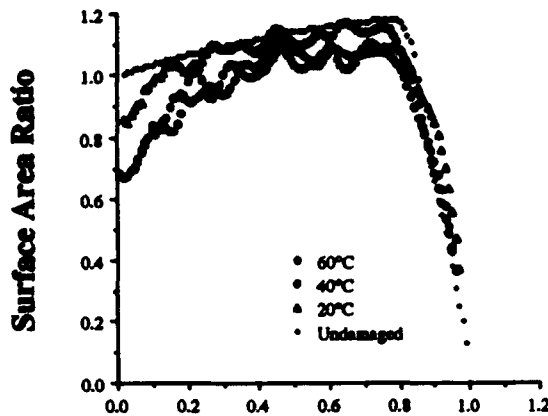
predict the failure modulus, as well. This allows for an estimate of the degree of damage and its effect on combustion for a wide variety of conditions, even those outside the area of possible physical measurement. If ballistic codes are used to show when certain surface area profiles subject a system to unacceptable performance, these equations can be used with the appropriate mechanical response parameters to predict when and where these conditions are likely to arise.

Other uses will become evident as the application or problem becomes more well defined. For a long time, the modeling community has had to rely on relatively arbitrary surface area augmentation algorithms. Now, for the first time, a method is available that relates a relatively easily determined mechanical parameter to a surface area profile during the early phase of combustion.

**5.2 Observations from Low Fracture Results** The experimental results for conditions in which the early grain deformation did not produce evidence of significant fracture during the early fraction burned were not included in the determination of the above equations. There were five such conditions and they are indicated by dashes in Table 2. However, those results did reveal interesting surface area profiles that were consistent with the data thus far reported and offer additional insight about the fracture process within the grains. The profiles that correspond to those five conditions, plus one other profile (20°C and 20% end strain) are shown in Figure 12.

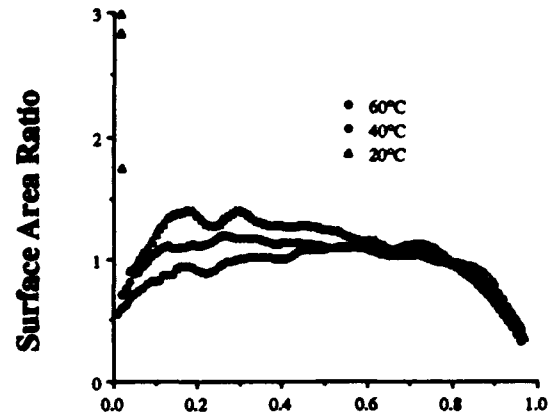
At higher temperatures and lower end strains, most of the deformation is plastic. This is reflected in Figure 12a by surface area values that are smaller than for undamaged grains. This type of surface area reduction has been observed in JA2 propellant that was uniaxially deformed in a completely plastic manner<sup>13</sup>. It is caused by the change of grain dimensions during propellant flow that resulted in less surface being made available to the flame. This can occur by an outright reduction in surface area or by perforations becoming blocked or pinched, thereby delaying the introduction of flame to that portion of the grain. Either mechanism reduces the progressivity of the grain. The profiles in this figure are for the 10% end-strain condition and at 60°C and 40°C, appear about the same. However, the 20°C profile shows a slightly higher profile for low fraction burned and lower progressivity as burning proceeded. This indicated that while plastic deformation was still the predominant failure mechanism, failure by fracture was beginning to influence the profile.

This is demonstrated more clearly in the 20% end-strain profiles in Figure 12b. Here, the loss of progressivity and the increase in available surface area (at 20% fraction burned) was marked. The onset of brittle fracture is indicated at 20°C by the large initial surface area, but the amount of fractured material was small as indicated by the immediate decrease in area. These three curves show that even though a large amount of fracture-generated surface area was not initially available to the



**Fraction Burned**

a. 10% End Strain



**Fraction Burned**

b. 20% End Strain

Figure 12. Surface Area vs. Fraction Burned for M30 Propellant with Low Fracture Response

flame, fracture surface area soon became available as combustion proceeded. This can occur through crack precursors creating cracks or the uncovering of existing fracture-damaged regions within the grain as the grain burns. In either case, the degree of fracture-related damage was increasing as temperature decreased and end strain increased, even before the grains displayed massive physical fracture. Figure 13 shows two typical grains that were compressed to 20% strain at 20°C. These grains show that the extent of visible fracture damage was small. Even so, the area profile showed the effects of increasingly brittle behavior.

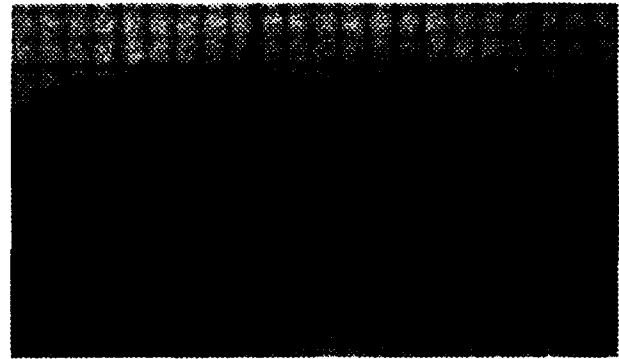


Figure 13. M30 Propellant Grains Compressed to 20% Strain at 20 °C (1-mm Divisions)

## 6. CONCLUSIONS

A correlation has been established that relates fracture-generated surface area to a mechanical parameter called the failure modulus and the end-state strain of uniaxially compressed propellant grains. The failure modulus has been shown in other studies to demonstrate a time-temperature equivalency that expands the application of these results to a wide variety of ballistic problems.

The effective surface area profile has been shown to be directly proportional to the logarithm of the failure modulus for each of the end-strain conditions tested, and the parameters determined in

these linear correlations (the constant and coefficient of each relationship) have been shown to be linear functions of the strain. The result of this is a method by which an equivalent surface area profile can be generated, based on the level of strain and the established failure modulus. It was also shown that the fracture process can have a demonstrated effect on the surface area profile even when most of the damage is from plastic flow. At high temperatures and low end strains, plastic deformation reduced the specific surface area. As more fracture damage occurs, the profile shows greater area available at low fraction burned and less progressivity. These results have wide application in the modeling and propellant development communities.

## 7. FUTURE STUDIES

This is the first propellant to undergo this series of tests. To verify the conclusions reached here, the test sequence should be repeated at other strains to see how those results compare with the ones presented here. If the conclusions are affirmed, similar methods of determination should then be performed for the three other major groups of propellants, i.e., single and double base propellants, and the nitramine composite formulations. This, along with the time-temperature equivalency established for each of these groups, should provide a valuable tool to predict the augmentation of pressure generation attributable to fracture damage in ballistic systems.

## 8. REFERENCES

1. Keller, G. E., and A. W. Horst. "The Effects of Propellant Grain Fracture on the Interior Ballistics of Guns." BRL-MR-3766, USA Ballistic Research Laboratory, Aberdeen Proving Ground, MD, June 1989.
2. Gazonas, G. A., A. Juhasz, and J. C. Ford. "Strain Rate Insensitivity of Damaged-Induced Surface Area in M30 and JA2 Gun Propellants." BRL-TR-3251, USA Ballistic Research Laboratory, Aberdeen Proving Ground, MD, August 1991.
3. Lu, P., B. Strauss, S. Moy, and R. Lieb. "Shaped Charge Jet Impact on Gun Propellants Study I - Temperature and Mechanical Properties Effects," 1991 Propulsion System Hazards Subcommittee Meeting, March 1991.
4. Lieb, R. J., and M. G. Leadore. "Mechanical Failure Parameters in Gun Propellants." BRL-TR-3296, USA Ballistic Research Laboratory, Aberdeen Proving Ground, MD, November 1991.
5. Gazonas, G.A. "The Mechanical Response of M30, XM39, and JA2 Propellants at Strain Rates from  $10^{-2}$  to  $250 \text{ sec}^{-1}$ ." BRL-TR-3181, USA Ballistic Research Laboratory, Aberdeen Proving Ground, MD, January 1991.
6. Lieb, R. J. "Impact-Generated Surface Area in Gun Propellants." BRL-TR-2946, USA Ballistic Research Laboratory, Aberdeen Proving Ground, MD, November 1988.
7. Lieb, R. J. "The Mechanical Response of M30, JA2 and XM39 Gun Propellants to High Rate Deformation." BRL-TR-3023, USA Ballistic Research Laboratory, Aberdeen Proving Ground, MD, August 1989.
8. Lieb, R. J. "High Strain Rate Response of Gun Propellant Using the Hopkinson Split Bar." BRL-TR-3200, USA Ballistic Research Laboratory, Aberdeen Proving Ground, MD, February 1991.
9. Varga, L., and F. Beaupre. "Temperature, Aging and Extrusion Pressure Effects on Mechanical Properties of LOVA Gun Propellants." DREV Memorandum 3072/92, Defence Research Establishment, Valcartier, Quebec, June 1992.
10. Lieb, R. J., and M. G. Leadore. "Mechanical Response Comparison of Gun Propellants Evaluated under Equivalent Time-Temperature Conditions." Proceedings of the 1992 JANNAF Structures & Mechanical Behavior Subcommittee Meeting, CPIA Publication 591, November 1992.

11. Lieb, R. J., and M. G. Leadore. "Time-Temperature Shift Factors for Gun Propellants." ARL-TR-131, Army Research Laboratory, Aberdeen Proving Ground, MD, May 1993.
12. Lieb, R. J., S. F. Trevino, and J. D. Barnes. "Onset and Nature of Fracture of Uniaxially Compressed Gun Propellants, *A Small-Angle Neutron and X-Ray Scattering Study*." ARL-TR-185, Army Research Laboratory, Aberdeen Proving Ground, MD, August 1993.
13. Lieb, R. J., D. Devynck, and J. J. Rocchio. "The Evaluation of High Rate Fracture Damage of Gun Propellant Grains." 1983 JANNAF Structure and Mechanical Behavior Subcommittee Meeting, CPIA Publication 388, November 1983.
14. Oberle, W. F., and D. E. Kooker. "BRLCB: A Closed-Chamber Data Analysis Program, *Part I - Theory and User's Manual*." ARL-TR-36, Army Research Laboratory, Aberdeen Proving Ground, MD, January 1993.

<u>No. of Copies</u>	<u>Organization</u>	<u>No. of Copies</u>	<u>Organization</u>
2	Administrator Defense Technical Info Center ATTN: DTIC-DDA Cameron Station Alexandria, VA 22304-6145	1	Commander U.S. Army Missile Command ATTN: AMSMI-RD-CS-R (DOC) Redstone Arsenal, AL 35898-5010
1	Commander U.S. Army Materiel Command ATTN: AMCAM 5001 Eisenhower Ave. Alexandria, VA 22333-0001	1	Commander U.S. Army Tank-Automotive Command ATTN: AMSTA-JSK (Armor Eng. Br.) Warren, MI 48397-5000
1	Director U.S. Army Research Laboratory ATTN: AMSRL-OP-CI-AD, Tech Publishing 2800 Powder Mill Rd. Adelphi, MD 20783-1145	1	Director U.S. Army TRADOC Analysis Command ATTN: ATRC-WSR White Sands Missile Range, NM 88002-5502
1	Director U.S. Army Research Laboratory ATTN: AMSRL-OP-CI-AD, Records Management 2800 Powder Mill Rd. Adelphi, MD 20783-1145	(Class. only) 1	Commandant U.S. Army Infantry School ATTN: ATSH-CD (Security Mgr.) Fort Benning, GA 31905-5660
2	Commander U.S. Army Armament Research, Development, and Engineering Center ATTN: SMCAR-IMI-I Picatinny Arsenal, NJ 07806-5000	(Unclass. only) 1	Commandant U.S. Army Infantry School ATTN: ATSH-WCB-O Fort Benning, GA 31905-5000
2	Commander U.S. Army Armament Research, Development, and Engineering Center ATTN: SMCAR-TDC Picatinny Arsenal, NJ 07806-5000	1	WL/MNOI Eglin AFB, FL 32542-5000
1	Director Benet Weapons Laboratory U.S. Army Armament Research, Development, and Engineering Center ATTN: SMCAR-CCB-TL Watervliet, NY 12189-4050		<u>Aberdeen Proving Ground</u>
1	Director U.S. Army Advanced Systems Research and Analysis Office (ATCOM) ATTN: AMSAT-R-NR, M/S 219-1 Ames Research Center Moffett Field, CA 94035-1000	2	Dir, USAMSAA ATTN: AMXSY-D AMXSY-MP, H. Cohen
		1	Cdr, USATECOM ATTN: AMSTE-TC
		1	Dir, ERDEC ATTN: SCBRD-RT
		1	Cdr, CBDA ATTN: AMSCB-CII
		1	Dir, USARL ATTN: AMSRL-SL-I
		5	Dir, USARL ATTN: AMSRL-OP-CI-B (Tech Lib)

<u>No. of Copies</u>	<u>Organization</u>
1	Chairman DOD Explosives Safety Board Room 856-C Hoffman Bldg. 1 2461 Eisenhower Avenue Alexandria, VA 22331-0600
1	Headquarters U.S. Army Materiel Command ATTN: AMCICP-AD, M. Fisette 5001 Eisenhower Ave. Alexandria, VA 22333-0001
1	U.S. Army Ballistic Missile Defense Systems Command Advanced Technology Center P.O. Box 1500 Huntsville, AL 35807-3801
1	Department of the Army Office of the Product Manager 155mm Howitzer, M109A6, Paladin ATTN: SFAE-AR-HIP-IP, Mr. R. De Kleine Picatinny Arsenal, NJ 07806-5000
3	Project Manager Advanced Field Artillery System ATTN: SFAE-ASM-AF-E, LTC A. Ellis T. Kuriata J. Shields Picatinny Arsenal, NJ 07801-5000
1	Project Manager Advanced Field Artillery System ATTN: SFAE-ASM-AF-Q, W. Warren Picatinny Arsenal, NJ 07801-5000
2	Commander Production Base Modernization Agency U.S. Army Armament Research, Development, and Engineering Center ATTN: AMSMC-PBM, A. Siklosi AMSMC-PBM-E, L. Laibson Picatinny Arsenal, NJ 07806-5000

<u>No. of Copies</u>	<u>Organization</u>
4	PEO-Armaments Project Manager Tank Main Armament System ATTN: AMCPM-TMA AMCPM-TMA-105 AMCPM-TMA-120 AMCPM-TMA-AS, H. Yuen Picatinny Arsenal, NJ 07806-5000
4	Commander U.S. Army Armament Research, Development, and Engineering Center ATTN: SMCAR-CCH-V, C. Mandala E. Fennell SMCAR-CCH-T, L. Rosendorf SMCAR-CCS Picatinny Arsenal, NJ 07806-5000
18	Commander U.S. Army Armament Research, Development, and Engineering Center ATTN: SMCAR-AEE, J. Lannon SMCAR-AEE-B, A. Beardell D. Downs S. Einstein S. Westley S. Bernstein J. Rutkowski B. Brodman P. O'Reilly R. Cirincione P. Hui J. O'Reilly SMCAR-AEE-WW, M. Mezger J. Pinto D. Wiegand P. Lu C. Hu SMCAR-AES, S. Kaplowitz Picatinny Arsenal, NJ 07806-5000
1	Commander U.S. Army Armament Research, Development and Engineering Center ATTN: SMCAR-HFM, E. Barriores Picatinny Arsenal, NJ 07806-5000

<u>No. of Copies</u>	<u>Organization</u>
9	<p>Commander U.S. Army Armament Research, Development and Engineering Center ATTN: SMCAR-FSA-F, LTC R. Riddle SMCAR-FSC, G. Ferdinand SMCAR-FS, T. Gora SMCAR-FS-DH, J. Feneck SMCAR-FSS-A, R. Kopmann B. Machek L. Pinder SMCAR-FSN-N, K. Chung Picatinny Arsenal, NJ 07806-5000</p>
3	<p>Director Benet Weapons Laboratories ATTN: SMCAR-CCB-RA, G.P. O'Hara G.A. Pflegl SMCAR-CCB-S, F. Heiser Watervliet, NY 12189-4050</p>
2	<p>Commander U.S. Army Research Office ATTN: Technical Library D. Mann P.O. Box 12211 Research Triangle Park, NC 27709-2211</p>
1	<p>Director Army Research Office ATTN: AMXRO-MCS, Mr. K. Clark P.O. Box 12211 Research Triangle Park, NC 27709-2211</p>
1	<p>Director Army Research Office ATTN: AMXRO-RT-IP, Library Services P.O. Box 12211 Research Triangle Park, NC 27709-2211</p>
1	<p>Commander, USACECOM R&amp;D Technical Library ATTN: ASQNC-ELC-IS-L-R, Myer Center Fort Monmouth, NJ 07703-5301</p>
1	<p>Commandant U.S. Army Aviation School ATTN: Aviation Agency Fort Rucker, AL 36360</p>

<u>No. of Copies</u>	<u>Organization</u>
1	<p>Program Manager U.S. Tank-Automotive Command ATTN: AMCPM-ABMS, T. Dean Warren, MI 48092-2498</p>
1	<p>Project Manager U.S. Tank-Automotive Command Fighting Vehicle Systems ATTN: SFAE-ASM-BV Warren, MI 48397-5000</p>
1	<p>Project Manager, Abrams Tank System ATTN: SFAE-ASM-AB Warren, MI 48397-5000</p>
1	<p>Director HQ, TRAC RPD ATTN: ATCD-MA Fort Monroe, VA 23651-5143</p>
1	<p>Commander U.S. Army Belvoir Research and Development Center ATTN: STRBE-WC Fort Belvoir, VA 22060-5006</p>
1	<p>Director U.S. Army TRAC-Ft. Lee ATTN: ATRC-L, Mr. Cameron Fort Lee, VA 23801-6140</p>
1	<p>Commandant U.S. Army Command and General Staff College Fort Leavenworth, KS 66027</p>
1	<p>Commandant U.S. Army Special Warfare School ATTN: Rev and Trng Lit Div Fort Bragg, NC 28307</p>
1	<p>Commander Radford Army Ammunition Plant ATTN: SMCAR-QA/HI LIB Radford, VA 24141-0298</p>

No. of Copies	Organization
1	Commander U.S. Army Foreign Science and Technology Center ATTN: AMXST-MC-3 220 Seventh Street, NE Charlottesville, VA 22901-5396
2	Commandant U.S. Army Field Artillery Center and School ATTN: ATSF-CO-MW, E. Dublisky ATSF-CN, P. Gross Ft. Sill, OK 73503-5600
1	Commandant U.S. Army Armor School ATTN: ATZK-CD-MS, M. Falkovitch Armor Agency Fort Knox, KY 40121-5215
1	U.S. Army Research Development and Standardization Group (UK) PSC 802 Box 15, Dr. Roy E. Richenbach FPO AE09499-1500
2	Commander Naval Sea Systems Command ATTN: SEA 62R SEA 64 Washington, DC 20362-5101
1	Commander Naval Air Systems Command ATTN: AIR-954-Tech Library Washington, DC 20360
4	Commander Naval Research Laboratory ATTN: Technical Library Code 4410, K. Kailasanate J. Boris E. Oran Washington, DC 20375-5000
1	Office of Naval Research ATTN: Code 473, R.S. Miller 800 N. Quincy Street Arlington, VA 22217-9999

No. of Copies	Organization
1	Office of Naval Technology ATTN: ONT-213, D. Siegel 800 N. Quincy St. Arlington, VA 22217-5000
2	Commander Naval Surface Warfare Center ATTN: Code 730 Code R-13, R. Bernecker Silver Spring, MD 20903-5000
7	Commander Naval Surface Warfare Center ATTN: T.C. Smith K. Rice S. Mitchell S. Peters J. Consaga C. Gotzmer Technical Library Indian Head, MD 20640-5000
4	Commander Naval Surface Warfare Center ATTN: Code G30, Guns & Munitions Div Code G32, Guns Systems Div Code G33, T. Doran Code E23 Technical Library Dahlgren, VA 22448-5000
5	Commander Naval Air Warfare Center ATTN: Code 388, C.F. Price T. Boggs Code 3895, T. Parr R. Derr Information Science Division China Lake, CA 93555-6001
1	Commanding Officer Naval Underwater Systems Center ATTN: Code 5B331, Technical Library Newport, RI 02840
1	AFOSR/NA ATTN: J. Tishkoff Bolling AFB, D.C. 20332-6448

<u>No. of Copies</u>	<u>Organization</u>
1	OLAC PL/TSTL ATTN: D. Shiplett Edwards AFB, CA 93523-5000
3	AL/LSCF ATTN: J. Levine L. Quinn T. Edwards Edwards AFB, CA 93523-5000
1	WL/MNAA ATTN: B. Simpson Eglin AFB, FL 32542-5434
1	WL/MNME Energetic Materials Branch 2306 Perimeter Rd. STE 9 Eglin AFB, FL 32542-5910
1	WL/MNSH ATTN: R. Drabczuk Eglin AFB, FL 32542-5434
2	NASA Langley Research Center ATTN: M.S. 408, W. Scallion D. Witcofski Hampton, VA 23605
1	Central Intelligence Agency Office of Intelligence Resources Room GA-07, HQS Washington, DC 20505
1	Central Intelligence Agency ATTN: J. Backofen NHB, Room 5N01 Washington, DC 20505
1	SDIO/TNI ATTN: L.H. Caveny Pentagon Washington, DC 20301-7100
1	SDIO/DA ATTN: E. Gerry Pentagon Washington, DC 21301-7100

<u>No. of Copies</u>	<u>Organization</u>
2	HQ DNA ATTN: D. Lewis A. Fahey 6801 Telegraph Rd. Alexandria, VA 22310-3398
1	Director Sandia National Laboratories Energetic Materials & Fluid Mechanics Department, 1512 ATTN: M. Baer P.O. Box 5800 Albuquerque, NM 87185
1	Director Sandia National Laboratories Combustion Research Facility ATTN: R. Carling Livermore, CA 94551-0469
1	Director Sandia National Laboratories ATTN: 8741, G. A. Beneditti P.O. Box 969 Livermore, CA 94551-0969
2	Director Lawrence Livermore National Laboratory ATTN: L-355, A. Buckingham M. Finger P.O. Box 808 Livermore, CA 94550-0622
2	Director Los Alamos Scientific Lab ATTN: T3/D. Butler M. Division/B. Craig P.O. Box 1663 Los Alamos, NM 87544
2	Battelle ATTN: TWSTIAC V. Levin 505 King Avenue Columbus, OH 43201-2693
1	Battelle PNL ATTN: M.C.C. Bampton P.O. Box 999 Richland, WA 99352

**No. of  
Copies    Organization**

- 1    Institute of Gas Technology  
ATTN: D. Gidaspow  
3424 S. State Street  
Chicago, IL 60616-3896
  
- 1    Institute for Advanced Technology  
ATTN: T.M. Kiehne  
The University of Texas at Austin  
4030-2 W. Braker Lane  
Austin, TX 78759-5329
  
- 2    CPIA - JHU  
ATTN: H. J. Hoffman  
T. Christian  
10630 Little Patuxent Parkway  
Suite 202  
Columbia, MD 21044-3200
  
- 1    Brigham Young University  
Department of Chemical Engineering  
ATTN: M. Beckstead  
Provo, UT 84601
  
- 1    Jet Propulsion Laboratory  
California Institute of Technology  
ATTN: L.D. Strand, MS 125/224  
4800 Oak Grove Drive  
Pasadena, CA 91109
  
- 1    California Institute of Technology  
204 Karman Lab  
Main Stop 301-46  
ATTN: F.E.C. Culick  
1201 E. California Street  
Pasadena, CA 91109
  
- 3    Georgia Institute of Technology  
School of Aerospace Engineering  
ATTN: B.T. Zim  
E. Price  
W.C. Strahle  
Atlanta, GA 30332
  
- 1    Massachusetts Institute of Technology  
Department of Mechanical Engineering  
ATTN: T. Toong  
77 Massachusetts Avenue  
Cambridge, MA 02139-4307

**No. of  
Copies    Organization**

- 2    University of Illinois  
Department of Mechanical/Industry  
Engineering  
ATTN: H. Krier  
R. Berdini  
144 MEB; 1206 N. Green St.  
Urbana, IL 61801-2978
  
- 1    University of Massachusetts  
Department of Mechanical Engineering  
ATTN: K. Jakus  
Amherst, MA 01002-0014
  
- 1    University of Minnesota  
Department of Mechanical Engineering  
ATTN: E. Fletcher  
Minneapolis, MN 55414-3368
  
- 3    Pennsylvania State University  
Department of Mechanical Engineering  
ATTN: V. Yang  
K. Kuo  
C. Merkle  
University Park, PA 16802-7501
  
- 1    Rensselaer Polytechnic Institute  
Department of Mathematics  
Troy, NY 12181
  
- 1    Stevens Institute of Technology  
Davidson Laboratory  
ATTN: R. McAlevy III  
Castle Point Station  
Hoboken, NJ 07030-5907
  
- 1    Rutgers University  
Department of Mechanical and  
Aerospace Engineering  
ATTN: S. Temkin  
University Heights Campus  
New Brunswick, NJ 08903
  
- 1    University of Southern California  
Mechanical Engineering Department  
ATTN: OHE200, M. Gerstein  
Los Angeles, CA 90089-5199

No. of Copies	Organization
1	University of Utah Department of Chemical Engineering ATTN: A. Baer Salt Lake City, UT 84112-1194
1	Washington State University Department of Mechanical Engineering ATTN: C.T. Crowe Pullman, WA 99163-5201
1	AFELM, The Rand Corporation ATTN: Library D 1700 Main Street Santa Monica, CA 90401-3297
1	Arrow Technology Associates, Inc. ATTN: W. Hathaway P.O. Box 4218 South Burlington, VT 05401-0042
3	AAI Corporation ATTN: J. Hebert J. Frankle D. Cleveland P.O. Box 126 Hunt Valley, MD 21030-0126
2	Alliant Techsystems, Inc. ATTN: R.E. Tompkins J. Kennedy 7225 Northland Dr. Brooklyn Park, MN 55428
1	Textron ATTN: A. Patrick 2385 Revere Beach Parkway Everett, MA 02149-5900
1	General Applied Sciences Lab ATTN: J. Erdos 77 Raynor Ave. Ronkonkoma, NY 11779-6649
1	General Electric Company Tactical System Department ATTN: J. Mandzy 100 Plastics Ave. Pittsfield, MA 01201-3698
1	IITRI ATTN: M.J. Klein 10 W. 35th Street Chicago, IL 60616-3799

No. of Copies	Organization
4	Hercules, Inc. Radford Army Ammunition Plant ATTN: L. Gizzi D.A. Worrell W.J. Worrell C. Chandler Radford, VA 24141-0299
2	Hercules, Inc. Allegheny Ballistics Laboratory ATTN: William B. Walkup Thomas F. Farabaugh P.O. Box 210 Rocket Center, WV 26726
1	Hercules, Inc. Aerospace ATTN: R. Cartwright 100 Howard Blvd. Kenville, NJ 07847
1	Hercules, Inc. Hercules Plaza ATTN: B.M. Riggelman Wilmington, DE 19894
1	MBR Research Inc. ATTN: Dr. Moshe Ben-Reuven 601 Ewing St., Suite C-22 Princeton, NJ 08540
1	Olin Corporation Badger Army Ammunition Plant ATTN: F.E. Wolf Baraboo, WI 53913
3	Olin Ordnance ATTN: E.J. Kirschke A.F. Gonzalez D.W. Worthington P.O. Box 222 St. Marks, FL 32355-0222
1	Olin Ordnance ATTN: H.A. McElroy 10101 9th Street, North St. Petersburg, FL 33716
1	Paul Gough Associates, Inc. ATTN: P.S. Gough 1048 South St. Portsmouth, NH 03801-5423

<u>No. of Copies</u>	<u>Organization</u>
1	Physics International Library ATTN: H. Wayne Wampler P.O. Box 5010 San Leandro, CA 94577-0599
2	Princeton Combustion Research Laboratories, Inc. ATTN: N. Mer N.A. Messina Princeton Corporate Plaza 11 Deerpark Dr., Bldg IV, Suite 119 Monmouth Junction, NJ 08852
3	Rockwell International Rocketdyne Division ATTN: BA08, J. Flanagan J. Gray R. Edelman 6633 Canoga Avenue Canoga Park, CA 91303-2703
2	Rockwell International Science Center ATTN: Dr. S. Chakravarthy Dr. S. Palaniswamy 1049 Camino Dos Rios P.O. Box 1085 Thousand Oaks, CA 91360
1	Science Applications International Corp. ATTN: M. Palmer 2109 Air Park Rd. Albuquerque, NM 87106
1	Southwest Research Institute ATTN: J.P. Riegel 6220 Culebra Road P.O. Drawer 28510 San Antonio, TX 78228-0510
1	Sverdrup Technology, Inc. ATTN: Dr. John Deur 2001 Aerospace Parkway Brook Park, OH 44142
3	Thiokol Corporation Elkton Division ATTN: R. Willer R. Biddle Tech Library P.O. Box 241 Elkton, MD 21921-0241

<u>No. of Copies</u>	<u>Organization</u>
1	Veritay Technology, Inc. ATTN: E. Fisher 4845 Millersport Hwy. East Amherst, NY 14501-0305
1	Universal Propulsion Company ATTN: H.J. McSpadden 25401 North Central Ave. Phoenix, AZ 85027-7837
1	SRI International Propulsion Sciences Division ATTN: Tech Library 333 Ravenwood Avenue Menlo Park, CA 94025-3493  <u>Aberdeen Proving Ground</u>
1	Cdr. USACSTA ATTN: STECS-PO/R. Hendricksen

## USER EVALUATION SHEET/CHANGE OF ADDRESS

This Laboratory undertakes a continuing effort to improve the quality of the reports it publishes. Your comments/answers to the items/questions below will aid us in our efforts.

1. ARL Report Number ARL-TR-307 Date of Report November 1993

2. Date Report Received \_\_\_\_\_

3. Does this report satisfy a need? (Comment on purpose, related project, or other area of interest for which the report will be used.) \_\_\_\_\_  
\_\_\_\_\_  
\_\_\_\_\_

4. Specifically, how is the report being used? (Information source, design data, procedure, source of ideas, etc.) \_\_\_\_\_  
\_\_\_\_\_  
\_\_\_\_\_

5. Has the information in this report led to any quantitative savings as far as man-hours or dollars saved, operating costs avoided, or efficiencies achieved, etc? If so, please elaborate. \_\_\_\_\_  
\_\_\_\_\_  
\_\_\_\_\_

6. General Comments. What do you think should be changed to improve future reports? (Indicate changes to organization, technical content, format, etc.) \_\_\_\_\_  
\_\_\_\_\_  
\_\_\_\_\_  
\_\_\_\_\_

### CURRENT ADDRESS

\_\_\_\_\_  
Organization

\_\_\_\_\_  
Name

\_\_\_\_\_  
Street or P.O. Box No.

\_\_\_\_\_  
City, State, Zip Code

7. If indicating a Change of Address or Address Correction, please provide the Current or Correct address above and the Old or Incorrect address below.

### OLD ADDRESS

\_\_\_\_\_  
Organization

\_\_\_\_\_  
Name

\_\_\_\_\_  
Street or P.O. Box No.

\_\_\_\_\_  
City, State, Zip Code

(Remove this sheet, fold as indicated, tape closed, and mail.)  
(DO NOT STAPLE)

---

**DEPARTMENT OF THE ARMY**



**OFFICIAL BUSINESS**

**BUSINESS REPLY MAIL**

**FIRST CLASS PERMIT No 0001, APG, MD**

Postage will be paid by addressee.

Director  
U.S. Army Research Laboratory  
ATTN: AMSRL-OP-CI-B (Tech Lib)  
Aberdeen Proving Ground, MD 21005-5066

**NO POSTAGE  
NECESSARY  
IF MAILED  
IN THE  
UNITED STATES**

